

Stability of a sonoluminescing nitrogen bubble in chilled water

Joachim Holzfuss¹ and Mogens T. Levinsen²

¹*Institut für Angewandte Physik, TU Darmstadt, Schloßgartenstraße 7, 64289 Darmstadt, Germany*

²*Complexity Lab, Niels Bohr Institute, Blegdamsvej 17, DK 2100 Copenhagen, Denmark*

(Received 24 October 2007; revised manuscript received 5 February 2008; published 8 April 2008)

Bubbles are levitated in a resonator driven by an ultrasound wave. Their highly nonlinear oscillations feature a strong collapse, where fluidlike densities and temperatures of several thousand degrees Kelvin are reached, resulting in the emission of ultrashort light pulses. Previous experiments and theories explained the observed stable bubble dynamic and emission on long time scales with the requirement of a noble gas. Recent experiments reveal stable sonoluminescent emission of nitrogen bubbles in chilled water without the presence of a noble gas. Numerical calculations show that a diffusive and dissociative equilibrium can be reached when the temperature within a nitrogen bubble is limited due to the presence of water vapor. Calculated stability lines agree with published experimental results. The results show that noble-gas-free stable single bubble sonoluminescence of nitrogen bubbles is possible.

DOI: [10.1103/PhysRevE.77.046304](https://doi.org/10.1103/PhysRevE.77.046304)

PACS number(s): 78.60.Mq

I. INTRODUCTION

Single bubble sonoluminescence (SBSL), the emission of a light pulse during collapse of a single bubble driven ultrasonically in water [1] is the consequence of the compression of the bubble at a main collapse [2]. The stability on a very long time scale of the repetitive phenomenon has been found to be the result of chemical dissociation of polyatomic, non-inert gases present within the bubble counteracting a rectified diffusive influx of air through the bubble boundary. Sonoluminescence in stably oscillating air seeded bubbles in water has been linked to a requirement of the presence of a noble gas (argon) [2]. Due to the enormous densities and temperatures during collapse, the noninert gases are dissociated and reaction products formed that are readily dissolved in the water. Only the inert argon remains.

It has been predicted earlier, that inert-gas-free stable sonoluminescence may be a possibility though [3]. Furthermore, experimental results were published for stable oscillations of nitrogen bubbles in water at ambient temperature [4]. Even earlier it has been reported, that very weak sonoluminescence is observed from unstably oscillating pure nitrogen bubbles [5,6]. However, the addition of a noble gas stabilizes the bubble and increases the light emission by orders of magnitude.

Recently it has been reported that stable SBSL is observed in pure nitrogen dissolved in chilled water [7]. A crucial point in obtaining this showed up to be a complete removal of inert gas (primarily argon) by repeated flushing with nitrogen over many hours. These experimental results show stably oscillating bubbles emitting weak light.

We present numerical calculations with a model of bubble oscillations to verify the existence and nature of these bubbles in different regions of the parameter space. The numerical model includes several aspects which we find are influencing the dynamics of nitrogen bubbles driven at high pressures. They are described in detail. Stability lines have been calculated in the relevant parameter region which are shown to agree with the experiment.

II. EXPERIMENT

In the experiment [7] a nitrogen bubble is levitated in a sealed cylindrical resonator cell, described in detail in [8]. The resonator is a quartz cylindrical cell of 21.930 kHz resonance frequency, 6 cm height and diameter, and metallic end caps. Piezoelectric transducers are mounted on both caps to deliver the driving pressure. The resonator is filled with distilled and degassed water. The water is furthermore filtered through a 0.2 micron particle filter, since particles are known to be caught by the oscillating bubble making the emission pattern anisotropic [9]. A specifiable concentration of nitrogen is dissolved in the water. Extreme care was taken to ensure that only nitrogen is present. A complete removal of inert gas (primarily argon) is achieved by repeated degassing and flushing with nitrogen over many hours in 15 min intervals. The temperature is set by locating the apparatus in a temperature controlled cooler.

A bubble is generated with the help of a heater wire. It is levitated in the center of the cell allowing the dynamical analysis of bubble radii, light pulse emission, and the determination of spectral temperatures. Data sets have been taken by Mie scattering of laser light by the oscillating bubbles and by calibrated stroboscopic images of the bubbles, which enables the detection of long term stability. Approximately 1000 data points per driving period are sampled to give a high resolution of the time evolution of the bubble radius. The stability is also checked by recording the intensity of every flash for hours. The driving pressure cannot be measured directly but has been determined from the experimental time evolution of the radius values by an optimal fit to the full model equations.

Finally, the spectrum is measured using an Ocean Optics QE65000 fiber based spectrometer calibrated in the 220–950 nm range by an Ocean Optics DH-2000-CAL NIST-traceable calibration source. The spectrum is collected using a quartz lens with the whole system being calibrated although there is no correction for absorption in the water and the quartz cell wall.

III. NUMERICAL MODEL

To describe a sonoluminescing bubble in a driving sound field one has to find equations for various aspects of this phenomenon. The radial oscillations of the bubble wall are described in Sec. III A. Due to the enormous compression the temperature in the bubble reaches very high values (Sec. III B). The bubble interior is modeled as a mixture of nitrogen and water vapor. The contents are dynamically changing due to gas diffusion (Sec. III C) and evaporation or condensation of water vapor (Sec. III D). Thermal effects lead to chemical dissociation of gas molecules (Sec. III E).

A. Radial oscillations

The Gilmore model [10] describing the radial motion of a bubble in a compressible liquid is integrated numerically.

$$\left(1 - \frac{\dot{R}}{C}\right)R\ddot{R} + \frac{3}{2}\left(1 - \frac{\dot{R}}{3C}\right)\dot{R}^2 = \left(1 + \frac{\dot{R}}{C}\right)H + \left(1 - \frac{\dot{R}}{C}\right)\frac{R}{C}\frac{dH}{dt}, \quad (1)$$

$$H = \int_{p_\infty}^{p(R,\dot{R})} \rho^{-1} dp, \quad \frac{p+B}{p_0+B} = \left\{\frac{\rho}{\rho_0}\right\}^n, \quad (2)$$

$$C = c|_{r=R} = \sqrt{\left.\frac{dp}{d\rho}\right|_{r=R}} = c_0 \left(\frac{p(R,\dot{R})+B}{p_0+B}\right)^{(n-1)/2n},$$

$$p(R,\dot{R}) = p_g(R) - \frac{2\sigma}{R} - \frac{4\eta}{R}\dot{R},$$

$$p_g(R) = \left(p_0 + \frac{2\sigma}{R_0}\right) \left(\frac{R_0^3 - b^3}{R^3 - b^3}\right)^\gamma \quad (3)$$

R is the bubble radius, and C , ρ , and $p(R,\dot{R})$ are the speed of sound in the liquid, its density, and the pressure at the bubble wall, respectively. The Tait equation is taken as the equation of state for water using $n=7.025$, $B=3046$ bars [11] as parameters. p_g is the pressure in the bubble. H is the enthalpy difference of the liquid at pressure p_∞ and $p(R,\dot{R})$ at the bubble wall. p_∞ is the pressure at infinity taken as $p_\infty = p_0 + p_A \cos(2\pi ft)$, $p_0 = 1.021$ atm increased by the hydrostatic pressure above the bubble. The driving frequency f is 21.93 kHz. The fluid parameters are from tabulated values [12,13]. b is a van der Waals hard-core radius and γ is a polytropic exponent.

B. Modeling temperature and density

The polytropic exponent γ in Eq. (3) is taken to be variable. Its value is set between 1 (=isothermal) and the adiabatic exponent of the gas according to an instantaneous Peclet number [3,14,15] $Pe = R_0^2 |\dot{R}(t)| / R(t) \kappa$, reflecting thermal conduction at the involved time scales. κ is the thermal diffusivity of the gas.

To avoid a change to isothermal behavior at the bubble wall turning point during maximum compression, the bubble

wall velocity is kept to its maximum during positive bubble accelerations at collapse. It is smoothly approaching the real velocity during the rest of the cycle. The adiabatic exponent γ is taken as an average over the values reflecting the instantaneous content of species, and is thus updated continuously. The value of the thermal diffusivity κ is taken as a variable, as it depends on the varying density ρ_g of the gas.

$$\kappa = \frac{k}{\rho_g c_p} = \frac{\rho_g(R_0)}{\rho_g(R)} 2 \times 10^{-5} \text{ m}^2 \text{ s}^{-1}. \quad (4)$$

k is the thermal conductivity and c_p is the specific heat at constant pressure. The value of κ is scaled with the ratio of ambient gas density to actual density.

The density in the bubble is calculated by

$$\rho_g(R) = \frac{n_{\text{total}} \bar{M}}{\frac{4}{3} \pi R^3}, \quad (5)$$

$$\frac{4}{3} \pi R^3 = \frac{n_{\text{total}} R_{\text{gas}} T_B}{p_g} + \frac{4}{3} \pi b^3, \quad (6)$$

where p_g is the pressure in the bubble, and $R_{\text{gas}} = 8.3143 \text{ J mol}^{-1} \text{ K}^{-1}$ is the gas constant. The van der Waals hard-core b is calculated as an average from the tabulated hard-core values and the number of moles of the i different gases, $i = \text{N}_2, \text{H}_2\text{O}$. \bar{M} is the molar mass averaged over all gases and n_{total} is the total number of moles. b and \bar{M} are updated continuously.

The temperature T_B is taken to be uniform within the bubble. It is calculated via the adiabatic compression of a van der Waals gas by

$$T_B = T_0 \left(\frac{R_0^3 - b^3}{R^3 - b^3}\right)^{\gamma-1}, \quad (7)$$

with the ambient liquid temperature T_0 . Other more complex approaches exist that include a temperature jump across the bubble interface [16,17].

C. Diffusion

Gas diffusion in the fluid may be described by an advection-diffusion equation in spherical symmetry

$$\frac{dC_i}{dt} = \frac{\partial C_i}{\partial t} + u \frac{\partial C_i}{\partial r} = D_i \frac{1}{r^2} \frac{\partial}{\partial r} \left(r^2 \frac{\partial C_i}{\partial r} \right). \quad (8)$$

D_i and C_i are the diffusion constants and concentration fields of the gas species $i = \text{N}_2$. u is the velocity of a fluid element which may be replaced by $u = R^2 \dot{R} / r^2$ (in the incompressible limit). The concentration of species at the bubble wall is assumed to connect to the partial pressures p_i inside according to Henry's law: $C_i|_{r=R} = C_i^0 p_i(R) / p_0$. The same law holds true for the concentrations at $r = \infty$.

The number of moles of nitrogen in the bubble n_i is changed by diffusion of nitrogen dissolved in the water through the bubble wall at radius R [3,18–20],

$$\dot{n}_i^{diff} = 4\pi R^2 \frac{1}{M_i} D_i \left. \frac{\partial C_i(r)}{\partial r} \right|_{r=R}. \quad (9)$$

M_i is the molar mass. The advective term with the transport velocity u in Eq. (8) can be eliminated by a moving reference frame [18,21,22]. Because of the slow diffusional time scale an adiabatic approximation [19,23,24] can be employed and the change per period T is

$$\frac{\Delta n_i^{diff}}{T} = \frac{4\pi D_i C_i^0 R_{max}}{M_i p_0} \left(p_i^\infty - \left\langle \frac{n_i}{n_0} p_g(R) \right\rangle_4 \right), \quad (10)$$

n_0 is the sum of moles of all molecules in the bubble, and

$$\langle f(t) \rangle_i = \frac{\int_0^T f(t) R^i(t) dt}{\int_0^T R^i(t) dt} \quad (11)$$

are weighted time averages. The gas contents in the bubbles are updated once per driving period according to Eq. (10).

D. Evaporation and condensation of water

Evaporation and condensation of water molecules at the bubble wall [2,17,25–27] are included in the model for the bubble dynamics, as experimental results [28,29] stress the importance of a decrease of the polytropic exponent induced by water vapor at bubble collapse. A simple Hertz/Knudsen model [30,31] for the change of moles n_{H_2O} of water vapor in the bubble is

$$\dot{n}_{H_2O} = \dot{n}_{H_2O}^{evap} - \dot{n}_{H_2O}^{cond} = \frac{4\pi R^2}{M_{H_2O}} \frac{\alpha \bar{c}(T_s)}{4} (\rho_{g,H_2O}^{sat} - \Gamma \rho_{g,H_2O}). \quad (12)$$

α is the constant evaporation coefficient (also called accommodation coefficient or sticking probability),

$$\bar{c}(T_s) = \sqrt{\frac{8R_{gas}T_s}{\pi M_{H_2O}}} \quad (13)$$

is the average velocity of molecules of a Maxwell-Boltzmann distribution, ρ_{g,H_2O} is the density of water vapor of molar weight M_{H_2O} in the bubble, and ρ_{g,H_2O}^{sat} is the saturated vapor density [12,13]. The bubble surface temperature is taken as $T_s = T_0$. The density of water vapor ρ_{g,H_2O} depends on the bubble dynamics and is calculated along with the bubble equation with the help of Eq. (5). The simple model (12) takes the temperature distributions in the bubble and liquid as fixed and does not capture all effects occurring during evaporation, as would do more complex treatments [32–34]. Γ is a correction factor for nonequilibrium conditions induced by mass motion of vapor and bubble wall movement (Schrage correction) [16,26,35].

$$\Gamma = e^{-\Omega^2} - \Omega \sqrt{\pi} \left(1 - \frac{2}{\sqrt{\pi}} \int_0^\Omega e^{-x^2} dx \right), \quad (14)$$

$$\Omega = \frac{\dot{R} - v_{H_2O}}{c_{peak}}. \quad (15)$$

Ω is a ratio of velocities, \dot{R} is the bubble wall velocity, v_{H_2O} is the vapor velocity, and c_{peak} is the velocity belonging to the peak of the Maxwell-Boltzmann velocity distribution.

$$c_{peak}(T_s) = \sqrt{\frac{2R_{gas}T_s}{M_{H_2O}}}. \quad (16)$$

The change of mass per unit time and unit area j can be expressed as

$$j = \frac{\dot{n}_{H_2O} M_{H_2O}}{4\pi R^2} = \rho_{g,H_2O} (\dot{R} - v_{H_2O}), \quad (17)$$

and when inserted into Eq. (15) leads to

$$\Omega = \frac{\dot{n}_{H_2O}}{n_{H_2O}} \frac{R}{3c_{peak}} \quad (18)$$

for a spherical bubble volume. For small values of Ω the approximation $\Gamma = 1 - \Omega \sqrt{\pi}$ can be made [35] leading to an effective constant evaporation coefficient of $\alpha_{eff} = 2\alpha / (2 - \alpha)$ in Eq. (12) and an effective correction factor Γ_{eff} of unity. Calculations show that Γ varies by as much as 20% around unity during the collapses. However, in the observed parameter range almost no notable difference exists in the amount of water vapor at collapse time between calculations using a constant value of α_{eff} and setting $\Gamma_{eff} = 1$, and calculations using Eq. (12) with the variable expressions (14) and (18) together with a smaller value of the evaporation coefficient $\alpha = 2\alpha_{eff} / (2 + \alpha_{eff})$. Therefore a constant value of α_{eff} [36] is taken in the following calculations.

E. Chemical dissociation

Chemical dissociation occurs for noninert gases [2,3,17,20,25,26,37–39]; reaction products are immediately diffused into the liquid, as all nitrogen reaction products have a high solubility in water. The dissociation per period of N_2 is calculated as a second order reaction by a modified Arrhenius law as follows:

$$\frac{\Delta n_i^{diss}}{T} = -n_i \langle [n_0] A_i T_B^{\beta_i} e^{-E_A^i / R_{gas} T_B} \rangle_0. \quad (19)$$

E_A^i are activation energies, $[n_0] = n_0 / \frac{4}{3} \pi R^3$ is the molar concentration of all molecules, and $i = N_2$. A_i and β_i are Arrhenius constants [40–42]. The braces denote the average per period [Eq. (11)].

A drop of the bubble temperature due to water vapor condensation and endothermic chemical reactions is neglected. The amount of water vapor at collapse is at most on the order of 10% and as the change of that amount caused by condensation around the highest temperature peak is $\approx \pm 5\%$, this contribution is small compared to the heating over a temperature range of several thousand degrees Kelvin. The same holds true for enthalpies of chemical reactions, as only $\approx 0.1\%$ of nitrogen molecules and 10% of water vapor are

dissociated during a single collapse. However, inclusion of these effects [17,37] would give a finer control over the results obtained here.

It is known that chemical dissociation of molecules at very high pressures does not follow Eq. (19) anymore. This feature has been described by the Lindemann-Hinshelwood expression [43], where the dependence of the dissociation rate with the pressure (or concentration) follows a nonlinear curve finally reaching a pressure independent rate. A more realistic expression uses a broadening factor F . In Eq. (19) the molar concentration of all molecules is replaced by an effective one, reflecting a gradual transition to pressure independence [44,45].

$$[n_0^{\text{eff}}] = \frac{[n_0]}{1 + \frac{[n_0]}{[n_\infty]}} F, \quad (20)$$

$$\log_{10} F = \left(\frac{1}{1 + \left\{ \log_{10} \frac{[n_0]}{[n_\infty]} \right\}^2} \right) \log_{10} F_c.$$

As the pressure independent rates or concentrations above which this occurs are unknown, the maximal possible concentration $[n_\infty]$ is taken as an upper threshold in the calculation of the rates. When all molecules are compressed to the hard-core b , the maximal achievable concentration is $[n_\infty] = n_0 / \frac{4}{3} \pi b^3$. The pressure dependence is then allowed to follow the modification in Eq. (20). As the hard-core is continuously updated during an oscillation, the overall rate depends on the size of hard-core, the temperature, the concentration of the dissociating molecule and, to a decreasing extent, on the overall concentration. $F_c = 0.6$ [45] is a fit parameter.

A rate reduction at high pressures, however, has not been implemented in all but one of the numerical calculations for the results presented here. The reason is that with the mentioned modifications [43–45] the dissociation rates are too small to dissociate an air bubble into an argon-vapor bubble at the usual parameters. Also, for calculations using parameters in the SBSL range and large initial values for the ambient bubble radius R_0 , unlimited growth by rectified diffusion is often observed in the calculations. This is not being backed up by current experimental observations. Other rate reduction mechanisms have been implemented [37,46] leading to the same observation in connection with this model framework. Rate reduction mechanisms have to be used with care because at the very high densities during collapse down to the hard-core the dissociation cannot keep up with the diffusive influx during the rest of the cycle.

IV. NUMERICAL RESULTS

A. Nitrogen bubbles in water at room temperature

Stability lines have been calculated at room temperature for different concentrations of nitrogen (Fig. 1). The lower three lines show the (unstable) diffusive stability curves corresponding to the unstable equilibrium curves denoted A in Lohse *et al.* [3]. Bubble parameters below the curves lead to

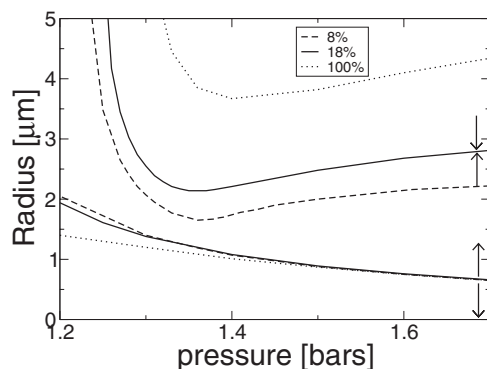


FIG. 1. Stability lines of nitrogen-vapor bubbles in water at different ambient gas concentrations and 20 °C. Shown is the ambient radius as a function of driving pressure at a hydrostatic pressure overhead of 3 cm water column and 21.930 kHz. The lower three lines show diffusive stability. The upper three lines show stability of diffusion and chemical dissociation. Attached to the 18% ambient concentration lines are arrows denoting the direction of bubble growth.

dissolution, and those above lead to growth. The upper three lines are stable equilibrium lines. Due to chemical dissociation the diffusive growth is counteracted and the bubble dynamics is stabilized. The stabilization sets in at higher values of the ambient radius with increasing nitrogen concentration. The model includes water vapor evaporation or condensation with an evaporation constant of 0.4 and no rate reduction mechanism [Eq. (20)]. The results show, that even at 100% nitrogen concentration bubbles could be stable. These stability curves are related to the stable equilibrium curves denoted B in [3]. However, in the case of an air bubble the position of these lines in parameter space are determined to a large extent by the dissociation due to collisions with argon atoms. In the present case where argon is absent, the nitrogen-nitrogen molecule collisions dominate resulting in a displacement of the stability curve with respect to the curve B of [3].

B. Nitrogen bubbles in chilled water

Experiments on pure nitrogen bubbles in water at lower temperatures have been done recently [7]. Measured radius-time curves have been compared against model calculations of the full model (Fig. 2). As the experiments have been conducted at 9 °C, all temperature dependent static parameters, such as surface tension and solubility, have been set accordingly [12]. The ambient pressure of 1.021 bars is augmented by the hydrostatic pressure in the cell above the bubble. The free parameters ambient radius and driving pressure of the model have been adjusted by minimizing the difference of numerical and experimental radius-time curves. Another requirement to fulfill is a diffusive-dissociative equilibrium on a long time scale. Resulting from this equilibrium criterion the evaporation coefficient is changed and the optimal value resulting in equilibrium can be determined ($\alpha = 0.14$, no rate reduction). A smaller evaporation coefficient results in larger amounts of water vapor at minimum collapse and thus lowers the maximum temperature

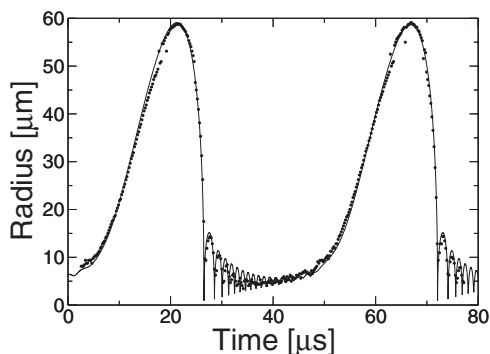


FIG. 2. Radius-time curve from experiment (dots) and numerical fit of a nitrogen bubble at 9 °C. The ambient radius has been determined to be 6 μm, the driving pressure 1.387 bars.

achieved. The opposite is true for larger values of α .

The lines in Fig. 3 show numerical results for different pairs of ambient radius and driving pressure in equilibrium. Details are shown as a function of the driving pressure (thick lines denoted “a”). Several properties have been calculated from the numerically determined fit values (lower graph of Fig. 3). The ambient radius shows large values, and they decrease with increasing driving pressure. The maximal radius, as seen in the experimental data, increases, as does the maximal temperature at collapse, calculated from the model. The amount of water vapor in the bubble at collapse increases to more than 50%. In all numerical curves, the higher pressure side is limited by parametric instability. To the left of the lower pressure side no equilibrium can be achieved, as the calculated collapse temperatures are too low to compensate for the diffusive influx.

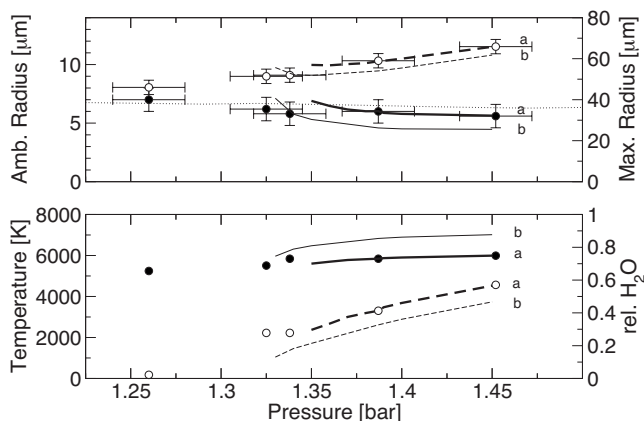


FIG. 3. Experimental data (dot connected circles) and numerical simulations (lines) of stable nitrogen-vapor bubbles in water at 18% ambient gas concentration and 9 °C. Top: Shown is the ambient radius (filled circles, straight lines) and maximal radius (hollow circles, dashed lines) as a function of driving pressure. Bottom: Temperature (filled circles, straight lines) and relative content of water vapor at bubble collapse minimum (hollow circles, dashed lines). The different numerical lines denote values obtained at diffusion-dissociation equilibrium, calculated with two different approaches: (a) evaporation coefficient $\alpha=0.14$ and (b) $\alpha=0.22$ including Lindemann/Hinschelwood correction. The thin dotted line shows values of ambient radius at the threshold of parametric instability, calculated according to approach “a”.

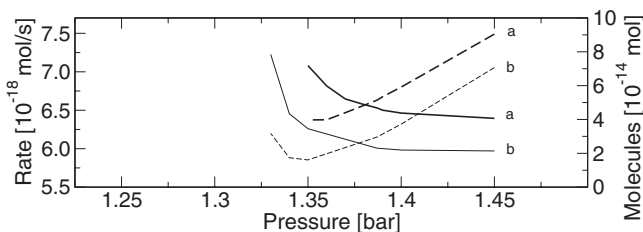


FIG. 4. Diffusion and dissociation rate of nitrogen at equilibrium (dashed lines) and the number of molecules of nitrogen (straight lines) in the bubble for the two different numerical approaches. The curves are labeled according to Fig. 3.

An evaporation coefficient of $\alpha=0.14$ optimally fits the higher pressure experimental data points (thicker lines in Fig. 3), whereas the lower pressure data points could only be fitted by higher values of α (resulting in less water vapor at collapse, higher temperatures, and increased dissociation of nitrogen). The calculated temperatures are lower than the spectral temperatures measured in [7].

The equilibrium lines of a slightly modified approach are seen in this graph as the thin lines denoted “b”. Here, the evaporation coefficient has been increased to $\alpha=0.22$ and the dissociation of nitrogen is limited due to the high pressures at collapse by the Lindemann/Hinschelwood correction (20). This results in higher calculated temperatures and in an acceptable fit of the experiments. The thin dotted line in Fig. 3 denotes the values of ambient radius at the onset of the parametric instability and surface mode oscillations. The calculated equilibrium lines are on the lower stable side denoting stability with regards to surface mode oscillations. The equilibrium lines are bounded by this instability. The bubbles exist, however, only rather close to the instability threshold.

The diffusion and dissociation rates of nitrogen at equilibrium are shown in Fig. 4 together with the number of molecules of nitrogen in the bubble. The rates are three to four orders of magnitude smaller than the available number of moles. Using the high pressure rate reduction (curves “b”) results in less nitrogen molecules and smaller rates at equilibrium.

Stable bubbles have also been measured at lower pressures than the numerical equilibrium lines would allow. The failure to numerically reproduce the lowest pressure data point can have several reasons: Diffusion and dissociation in these experimental bubbles may effectively not be in a stable equilibrium. They can be on the (unstable) diffusive equilibrium line and grow or shrink on a very long time scale. As the dissociation model and the evaporation model are, in fact, based on approximations and the Arrhenius parameters for dissociation and the evaporation coefficient are based on estimates and recommendations, it is surprising that the higher pressure experimental data points can be modeled reasonably well. The usage of a rate reduction mechanism like Eq. (20) seems to be justified as the calculated temperatures at diffusive-dissociative equilibrium agree better with the spectral temperatures observed in experiments [7,47].

V. BUBBLE LIGHT EMISSION

The spectrum of the stable nitrogen bubble was also measured in [7] using a crude spectrometer made of seven pho-

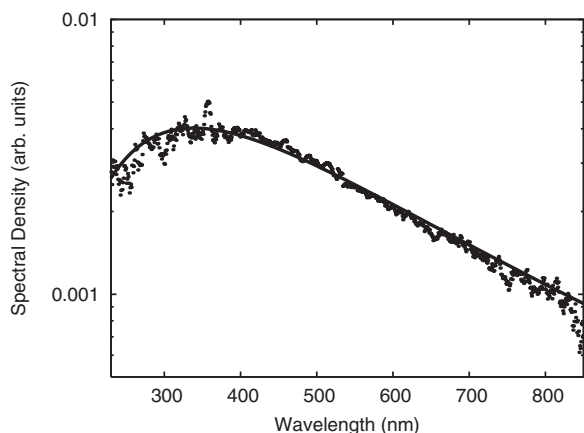


FIG. 5. Measured spectrum of light emission from a stable nitrogen bubble (dots) and calculated blackbody spectrum of 8500 K.

tomultiplier tubes fronted by narrow band (10 nm) optical filters. The spectrum was measured relative to that of an argon bubble. For easy characterization by one parameter it was assumed that the spectrum of the argon bubble could be fitted to blackbody radiation at 14 000 K. Compared to this, the nitrogen bubble spectrum looks much colder and is of the order of 8500 K. This naturally does not imply that the emission is blackbody radiation.

We have repeated this measurement using a commercial spectrometer. A calibrated sample spectrum (300 s integration time) is displayed in Fig. 5. The temperature of the cell is 9 °C and the relative concentration of nitrogen is 0.18 as in [7]. The spectrum is taken at the highest level of sound pressure for which the bubble is still stable. As before the spectrum looks very much like blackbody radiation from an 8500 K source.

Following Brenner *et al.* [2] we assume that the emission can be modeled by volume emission (in the transparent limit, where the optical thickness $\tau \ll 1$)

$$P_{\lambda}^{\text{thin}} d\lambda \approx \tau P_{\lambda}^{\text{Pl}}[T(t)] d\lambda, \quad (21)$$

where $P_{\lambda}^{\text{Pl}}[T(t)]$ is the Planck blackbody radiation, and local thermal equilibrium has been assumed. As xenon

has approximately the same ionization energy as nitrogen (~ 14.5 eV), xenon offers the best possibility for a comparison. In the case of nitrogen, the bubble size and temperature given from the model is determined by the requirement of balancing the influx of nitrogen molecules with the burn off and subsequent removal of reaction products with water vapor playing an indirect role. This temperature is found to be approximately 6500 K. For a xenon bubble the bubble temperature becomes much higher due to the larger gamma factor for noble gases with the most important factor limiting the temperature being the dissociation of water molecules.

Where about 10% of the xenon is expected to be ionized (see [2]), the corresponding ionization level for nitrogen is certainly much lower. It is therefore fair to assume that the nitrogen bubble is much more transparent to its own emission at all wavelengths than a xenon bubble. From this argument the relative prefactor in a fit to blackbody radiation should be much lower for nitrogen than for xenon. Indeed, it is lower by a factor of 30–40 which seems to vindicate the argument. A much more careful analysis is of course needed in order to verify this understanding, since unknown factors such as the precise size of the nitrogen bubble at the time of the collapse and also the pulse length of the emission do play a role in determining the prefactor.

VI. CONCLUSION

A numerical model of a nitrogen bubble in chilled water driven by ultrasound is presented. It models the radial oscillations of the bubble, the diffusional influx of nitrogen and its removal by high pressure chemical dissociation, and the evaporation and condensation of water vapor in the bubble. Numerical diffusive-dissociative stability lines are calculated that agree with recent experimental findings. It is shown that stability is achieved by the presence of water vapor in the bubble. The vapor limits the temperature by decreasing the average polytropic exponent and suppresses complete dissociation of nitrogen. These findings in accordance with experiments show that stable single bubble sonoluminescence is possible without the presence of an inert gas.

- [1] D. F. Gaitan, L. A. Crum, C. C. Church, and R. A. Roy, *J. Acoust. Soc. Am.* **91**, 3166 (1992).
 [2] M. P. Brenner, S. Hilgenfeldt, and D. Lohse, *Rev. Mod. Phys.* **74**, 425 (2002).
 [3] D. Lohse and S. Hilgenfeldt, *J. Chem. Phys.* **107**, 6986 (1997).
 [4] J. A. Ketterling and R. E. Apfel, *Phys. Rev. Lett.* **81**, 4991 (1998).
 [5] R. Hiller, K. Weninger, S. J. Putterman, and B. P. Barber, *Science* **266**, 248 (1994).
 [6] B. P. Barber, R. A. Hiller, R. Löfstedt, S. J. Putterman, and K. R. Weninger, *Phys. Rep.* **281**, 65 (1997).
 [7] M. T. Levinsen and J. S. Dam, *Europhys. Lett.* **80**, 27004 (2007).
 [8] M. T. Levinsen, N. Weppenaar, J. S. Dam, G. Simon, and M.

Skogstad, *Phys. Rev. E* **68**, 035303(R) (2003).

- [9] J. S. Dam and M. T. Levinsen, *Phys. Rev. Lett.* **92**, 144301 (2004).
 [10] F. R. Gilmore, Hydrodynamics Laboratory, California Institute of Technology Report No. 26-4, 1952 (unpublished).
 [11] J. Holzfuß, M. Rüggeberg, and A. Billo, *Phys. Rev. Lett.* **81**, 5434 (1998).
 [12] At 9 °C the following parameters have been taken in the calculations: surface tension $\sigma=0.0743$ N m⁻¹, viscosity $\eta=0.001346$ N s m⁻², saturated vapor density $\rho_{g,H_2O}^{\text{sat}}=0.00882$ kg m⁻³, diffusion constant $D_{N_2}=1.29 \times 10^{-9}$ m² s⁻¹, solubility $N_2=0.02418$ kg m⁻³, and water density $\rho=999.85$ kg m⁻³.
 [13] At 20 °C the following parameters have been taken in the

- calculations: surface tension $\sigma=0.0725$ N m⁻¹, viscosity $\eta=0.001$ N s m⁻², saturated vapor density $\rho_{g,H_2O}^{sat}=0.0173$ kg m⁻³, diffusion constant $D_{N_2}=1.9\times 10^{-9}$ m² s⁻¹, solubility $N_2=0.020$ kg m⁻³, water density $\rho=998.23$ kg m⁻³, and sound velocity $c=1483$ m s⁻¹.
- [14] A. Prosperetti, *J. Acoust. Soc. Am.* **61**, 17 (1977).
 [15] M. S. Plesset and A. Prosperetti, *Annu. Rev. Fluid Mech.* **9**, 145 (1977).
 [16] K. Yasui, *J. Acoust. Soc. Am.* **98**, 2772 (1995).
 [17] K. Yasui, *J. Phys. Soc. Jpn.* **66**, 2911 (1997).
 [18] R. Löfstedt, B. P. Barber, and S. J. Putterman, *Phys. Fluids A* **5**, 2911 (1993).
 [19] M. M. Fyrillas and A. J. Szeri, *J. Fluid Mech.* **277**, 381 (1994).
 [20] D. Lohse, M. P. Brenner, T. F. Dupont, S. Hilgenfeldt, and B. Johnston, *Phys. Rev. Lett.* **78**, 1359 (1997).
 [21] M. S. Plesset and S. A. Zwick, *J. Appl. Phys.* **23**, 95 (1952).
 [22] A. Eller and H. G. Flynn, *J. Acoust. Soc. Am.* **37**, 493 (1965).
 [23] R. Löfstedt, K. R. Weninger, S. Putterman, and B. P. Barber, *Phys. Rev. E* **51**, 4400 (1995).
 [24] S. Hilgenfeldt, D. Lohse, and M. P. Brenner, *Phys. Fluids* **8**, 2808 (1996).
 [25] V. Kamath, A. Prosperetti, and F. N. Egolfopoulos, *J. Acoust. Soc. Am.* **94**, 248 (1993).
 [26] B. D. Storey and A. J. Szeri, *Proc. R. Soc. London, Ser. A* **456**, 1685 (2000).
 [27] B. D. Storey and A. J. Szeri, *Phys. Rev. Lett.* **88**, 074301 (2002).
 [28] G. E. Vazquez and S. J. Putterman, *Phys. Rev. Lett.* **85**, 3037 (2000).
 [29] R. Toegel, B. Gompf, R. Pecha, and D. Lohse, *Phys. Rev. Lett.* **85**, 3165 (2000).
 [30] H. Hertz, *Ann. Phys.* **17**, 178 (1882).
 [31] M. Knudsen, *Kinetic Theory of Gases* (Methuen and Co., London, 1950).
 [32] M. Bond and H. Struchtrup, *Phys. Rev. E* **70**, 061605 (2004).
 [33] D. J. E. Harvie and D. F. Fletcher, *J. Heat Transfer* **123**, 486 (2001).
 [34] G. Hauke, D. Fuster, and C. Dopazo, *Phys. Rev. E* **75**, 066310 (2007).
 [35] R. W. Schrage, *A Theoretical Study of Interphase Mass Transfer* (Columbia University Press, New York, 1953).
 [36] I. W. Eames, N. J. Marr, and H. Sabir, *Int. J. Heat Mass Transfer* **40**, 2963 (1997).
 [37] R. Toegel and D. Lohse, *J. Chem. Phys.* **118**, 1863 (2003).
 [38] L. S. Bernstein, M. R. Zakin, E. B. Flint, and K. S. Suslick, *J. Phys. Chem.* **100**, 6612 (1996).
 [39] A. J. Colussi, L. K. Weavers, and M. R. Hoffmann, *J. Phys. Chem. A* **102**, 6927 (1998).
 [40] Arrhenius constants: $A_i=2.3\times 10^{23}$ m³ mol⁻¹ s⁻¹, $\beta_i=-3.5$, $E_A^i/R_{gas}=113\ 200$ K for nitrogen dissociation, from Ref. [48].
 [41] NIST kinetics database, <http://kinetics.nist.gov>.
 [42] D. L. Baulch, D. D. Drysdale, and D. G. Horne, *Evaluated Kinetic Data for High Temperature Reactions* (Butterworths, London, 1972), Vol. 2.
 [43] W. C. Gardiner and J. Troe, in *Combustion Chemistry*, edited by W. C. Gardiner (Springer Verlag, New York, 1984), Chapt. 4.
 [44] J. Troe, *J. Phys. Chem.* **83**, 114 (1979).
 [45] S. Sander, R. R. Friedl, D. M. Golden, M. J. Kurylo, R. E. Huie, V. L. Orkin, G. K. Moortgat, A. R. Ravishankara, C. E. Kolb, M. J. Molina, and B. J. Finlayson-Pitts, NASA Panel for Data Evaluation, Evaluation No. 14, JPL Publication No. 02-25 (2003).
 [46] J. Holzfuss, *Phys. Rev. E* **71**, 026304 (2005).
 [47] In Ref. [7] numerical simulations showed agreement with different experimental data. The authors used a modified RP equation [18], dissociation rules based on Ref. [49,50], and a high pressure rate reduction as in Ref. [46]. As those nitrogen dissociation rates are smaller up to a factor of 4 in the relevant temperature range, a higher temperature and dissociation rate to balance rectified diffusion is achieved by assuming less water vapor at collapse by fixing the accommodation coefficient to $\alpha=0.4$.
 [48] D. J. Kewley and H. G. Hornung, *Chem. Phys. Lett.* **25**, 531 (1974).
 [49] S. Byron, *J. Chem. Phys.* **44**, 1378 (1966).
 [50] G. F. Punte and F. J. Bonetto, *Phys. Rev. E* **71**, 056309 (2005).